Experimental And Finite Element Studies of Stretch Forming Process for AA2014 Alloy At Elevated Temperature

Kosaraju Satyanarayana[1*], *Kuraku* Ratna Babu[1], *Dharavath* Baloji[2], *Sriramoji* Vilas Chary[1], *Chintha* Pranay Kumar[1], *Dodda* Yaswanth Chowdary[1], *M. Abdulfadhil* Gatea[3,4], *Ishteyaaq* Ahmad[5]

[1]Department Of Mechanical Engineering, Gokaraju Rangaraju Institute Of Engineering And Technology, Hyderabad 500090, India.
[2]Department Of Mechanical Engineering, KG Reddy College of Engineering And Technology, Hyderabad 500072, India.
[3] Technical Engineering Department College of Technical Engineering, The Islamic University, Najaf, Iraq
[4] Department of Physics, College of Science, University of Kufa.
[5] Uttaranchal School of Computing Sciences, Uttaranchal University, Dehradun 248007 INDIA

Abstract: Sheet metal forming operations play a crucial role in the manufacturing process of various products. However, the challenge of plastic instability, which often leads to defective products, continues to persist in this field. It is important to consider various parameters, such as the Forming Limit Diagram (FLD), to overcome this issue during manufacturing. The Aluminium Alloy (AA2014) has been employed in this study to investigate its formability under different temperatures (room temperature, 150 ℃, and 300 ℃) at the strain rate of 0.1mm/s. The results of the study were obtained by performing stretch forming by utilizing the Nakajima test. The results showed the limiting strains of the material improved with an increase in temperature, and the findings were analyzed through fractography studies performed with a Scanning electron microscope, and simulations were done using LS-dyna software. This study provides valuable insights into the formability of AA 2014 sheets at elevated temperatures and will aid in the development of more efficient and effective sheet metal forming operations.

1 Introduction

Aluminium alloys are used in several industries due to their unique characteristics, including low weight, high thermal conductivity, and good formability. These attributes make aluminium alloys suitable for producing lightweight and high-performance components in applications like aerospace and automotive. Aluminium has been extensively utilized in

* Corresponding author: satyanarayana.kosaraju@gmail.com

structural applications for many years because of its distinct characteristics. This material is strong yet lightweight, has outstanding resistance to corrosion, and possesses good thermal conductivity. These alloys are good due to their low density and impressive ability to resist corrosion, which makes them suitable for use in the automotive and aerospace sectors [1]. Since the beginning of commercial aircraft manufacturing, Aluminium 2XXX alloys have been commonly used in the aircraft industry. The first alloy that was used for aircraft design was Al-Cu-Mg alloy, which is also known as Duralumin. The primary strengthening process in 2XXX aluminium alloys is precipitation hardening [2]. The 2xxx series of aluminium alloys have copper as the main component, with minor amounts of magnesium and manganese included. This composition offers the alloy high strength, excellent ability to be shaped, and good machinability. The strength comes from the reaction between copper and magnesium that causes precipitation hardening. These alloys are known for their exceptional resistance to corrosion in both acidic and alkaline environments. This feature makes them suitable for use in aerospace structures and other components that need to be protected from corrosion. The 2xxx series of alloys are suitable for applications requiring intricate shapes and precise tolerances due to their high formability. They are also adaptable to heat treatment, which increases their mechanical properties. This makes the alloys ideal for use in applications like aircraft skins and hydraulic systems [3-4].

The Al-4.5%Cu alloy (AA2014) aluminium alloy, which contains 4.5% copper, is frequently employed in the aerospace and automotive sectors because it offers a combination of high strength-to-weight ratio and excellent machinability. Its ability to maintain strength at elevated temperatures makes it a popular choice for components that operate in high-temperature environments such as airframes and engine components. Several research studies have concentrated on examining how alloying elements affect the precipitation behaviour of aluminium alloys and change properties, their performance, and their behaviour under conditions of fatigue and creep. [5-6]. Abass Ali Saleh, [7] conducted a study on the impact of heat treatment on AA2014 alloy and findings showed that the optimal solutionzing temperature was 513°C. When the temperature was below 503°C, there was a tendency for the hardness to increase with a longer soaking time. Ashok et.al, [8] conducted a study on the mechanical properties of AA2014 alloy through hot tensile testing at six different temperatures, ranging from room temperature to 300℃ and found that the higher yield strength and ultimate tensile strength observed at lower temperatures due to sub-grain formation during the deformation process. Anoop Kumar Pandouria et.al**,** [9] investigated the mechanical behaviour of AA2014-T6 alloy subjected to compression and tension loading under both quasi-static and dynamic conditions. They examined the effect of strain rates ranging from (10^{-4} to 2×10^{3} s^{-1}) and temperatures (25 °C to 250 °C) and concluded that the plastic flow stress of the material exhibited positive strain rate sensitivity across a wide range of strain rates for both types of loading.

Sheet metal formability refers to a metal's ability to be moulded into a specific shape without breaking or thinning out excessively. However, each sheet metal has a limit to how much it can be deformed, known as the forming limit curve (FLC). The FLC is typically affected by localized necking, which can lead to ductile fracture. The FLC is graphed as the major strain (ε_1) at the onset of localized necking for all minor strain values (ε_2), and this graph is called the forming limit diagram (FLD). The FLC is divided into two branches: the "left branch" and the "right branch." The right branch applies to positive major and minor strains, while the left branch is relevant to positive major and negative minor strains. The FLC only applies

to proportional strain paths, and various major and minor strain ratios are used to create the FLC. Strain paths on the "left side" range from uniaxial tension to plane strain, while strain ratios on the "right branch" differ from plane strain to full biaxial stretching. Figure 1 illustrates the forming limit diagram [10-11].

Hussaini et.al, [12] performed stretch forming of ASS 316 using a hemispherical punch for a temperature range from room temperature (RT) to 400 and plotted experimental FLD. They created an experimental forming limit diagram (FLD) and compared it to a theoretical FLD predicted using the Marciniak-Kuczynski model. Their findings showed that major strain was predominant in the FLD and that the onset of dynamic strain aging (DSA) was a critical factor in determining the metal's formability. Xugang Wang et.al,[13] determined the cryogenic forming limit of 6061 aluminium alloy and concluded that The forming limit of AA6061 tube at −196 °C is approximately double that at room temperature, especially in the tension-tension zone, which contributes significantly to the forming of complex features under biaxial tension. Pavan Kumar et.al, [14] determined formability of steel,brass with different tests available like Fukui's Conical Cup Drawing Test, Swift Cu etc and compared them. Nejia Ayachi et.al, [15] developed Nakazima test suitable for determining formability of thin copper sheets and findings indicate FLCs that obtained by Nakazima test are similar to those obtained through the reference Marciniak approach, resulting in a low value of major strain that approaches a plane strain state. Venugopal et.al, [16] investigated the forming behaviour of AA2014 thin tubes and concluded that radial expansion in tubes increase as the temperature increases.

Nitin Kotkund et.al, [17] performed finite element analysis on Ti-6Al-4V alloy at 400 ℃ for stretch forming by using DYNAFORM software with LS-DYNA server and compared with experimental results and It has been observed that Barlat 1989 yield criterion prediction is more accurate than Hill 1948. Lumelskyj et.al, [18] utilized finite element analysis to create FLCs for six specimens of varying widths (30, 50, 60, 77, and 99 mm) as well as one full circular specimen with a diameter of 110 mm. The specimens were divided into finite element meshes with an element size of h = 0.5 mm in the central region where failure was expected. Nakazima test model was employed for simulations, assuming a constant punch velocity of 1 m/s. The authors concluded that comparing the numerical results to the experimental FLC confirmed the feasibility of using finite element simulations to determine FLCs. Sreenath et.al, [19] generated FLD for AA2014 and AA2024 by using the nakazima test simulation tool and compared experimental results with simulations results and They validated the simulation tool. As there is a strong concurrence between the FLCs generated through experimental means and software, indicating good agreement. J.J.S. Dilip et.al, [20] through their investigation observed that the consumable rods of alloy 2014-T6 were observed to have microstructures consisting of highly elongated grains containing a significant number of second-phase particles (ranging from 5 to 10 μm in size) that were aligned in the working direction. Using SEM-EDS analysis, it was confirmed that these particles were Al2Cu and Fe-Mn-Al On the other hand, examining the friction deposit in its as-deposited condition via SEM revealed very fine, equiaxed grains that were less than 3 μm in size. The grain size appeared to be consistent across the layers, indicating that reheating effects did not cause grain coarsening.

In the past, the formability of AA 2014 tubes was carried out at an evaluated temperature and the microstructure analysis has been done the outcome of the study is telling the formability of sheets and radial expansion in tubes increase as the temperature increases in

this current study, FLD plotted at evaluated temperatures (room temperature, 150℃, 300℃) with a strain rate of 0.1mm/s. The fractography investigations conducted with a scanning electron microscope and FLD generated by simulations and experimental is compared.

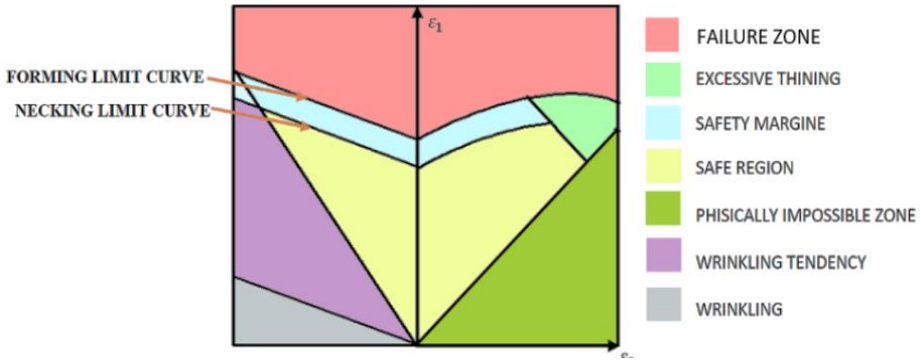

Fig.1. Forming limit diagram.

2 Experimental details

2.1 Material specifications

In this study, a 1.0-millimeter-thick sheet of AA 2014 was employed as the material of interest. The chemical composition of the AA 2014 sheet metal was examined and recorded in Table 1. This alloy contains 4.5% Copper and is a useful element in AA 2014 aluminium alloy because it increases the material's strength, hardness, and resistance to wear and corrosion. and increases the alloy's ability to withstand high temperatures and also improves its electrical conductivity.

Table 1. Chemical composition of AA2014 sheet

Element	Composition (wt.%)
Al	92.96
Cu	4.519
Mg	0.599
Fe	0.133
Ti	0.019
Zn	0.045
Mn	0.756
Si	0.897
Cr	0.006
Other Elements	0.065

2.2 Nakazima Test (Hemispherical Dome test) for Stretch Forming

The study involved stretching the AA2014 material using a 20-ton hydraulic press, which had a 2-zone split furnace and temperature controller to maintain a consistent temperature with ± 3% accuracy and it as Servo controlled force and displacement, Speed range 0.00001mm/min to 250mm/mi. The stretching apparatus included a 50mm diameter hemispherical dome-shaped punch, and the blank holder plate had a grooved bead to restrict material flow into the cavity. Various specimens of different widths were used, and the stretching setup was shown in Figure 2. The experiment involved laser etching circular grids with a diameter of 2.5mm on the blanks to measure strains using a travelling electron microscope after the stretching operation. The experiment was performed at three different temperatures (room temperature, 150°C, and 300°C) with a punch speed of 0.1mm/s. three different types of specimens (Figure 3(a)-(c)) were used to plot the forming limit diagram (FLD) in this study.

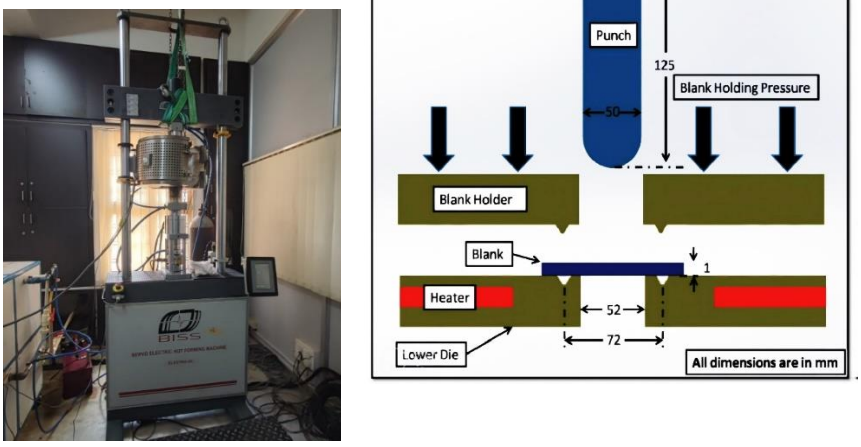

a) b)

Fig.2. a) Experimental setup; b) Schematic Diagram

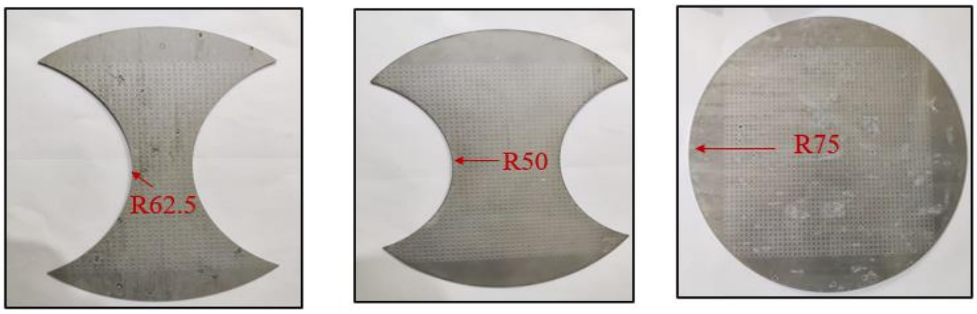

a) b) c)

Fig.3. specimens for Nakazima test a) R62.5; b) R50; c) R75

3 Simulations

3.1 Mesh generation and 3D modelling

The process of analyzing through FE (finite element) simulation involves the creation of models for the necessary tools and appropriately meshing them. In this study, the geometries of the tools and blank were created using solid works and saved in STEP File format. These meshes were then imported into LS-Dyna. Once the meshing was complete, initial and boundary conditions, as well as process parameters, were defined. The blank was designated as the deformable body, while the other tools were considered rigid bodies.

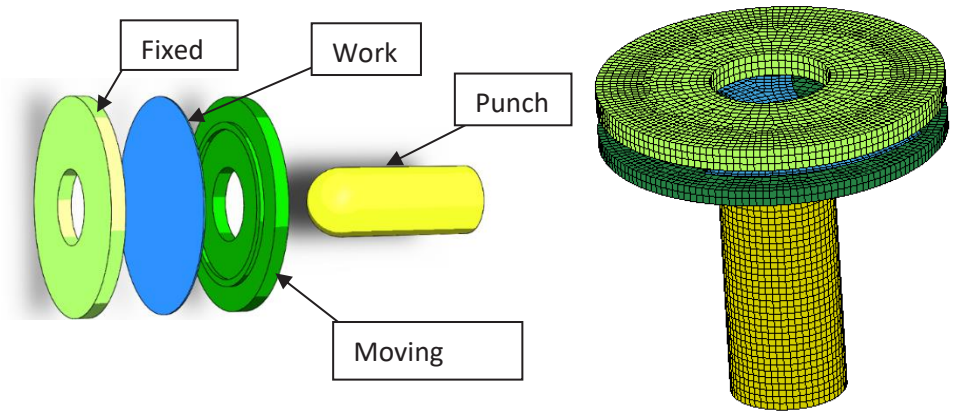

Fig.4. a) 3D model for stretch forming; b) Finite element model.

3.2 FE Simulations

Finite Element Analysis (FEA) is a technique for simulating and studying the behaviour of materials and structures when subjected to different loading conditions. The process involves breaking down the material or structure into smaller, simpler parts called finite elements, and solving the equations that govern the behaviour of each element. The results of these equations can then be used to predict the behaviour of the material or structure as a whole when subjected to various loading conditions. FEA simulations are particularly useful for analysing complex structures or materials, such as aluminium alloy 2014, where predicting behaviour using analytical methods is challenging. These simulations can model a broad range of physical phenomena, including deformation, stress, strain, and thermal behaviour. The overall performance of a material or structure is forecasted by amalgamating the outcomes of each individual component. This approach can offer a significant understanding of how the material or structure will respond to diverse types of stress, like temperature variations, pressure alterations, or mechanical strains. The process parameters and the material properties taken from simulations are shown in table 2 and table 3.

Table 2. Material properties taken for simulations.

YS (MPa)	Failure criteria	Elastic modulus (MPa)	r	N	Poisson's ratio (pr)	Mass density (kg/m^3)
463.802	0.18	7308	0.68	0.171	0.330	2795

Table 3. Process Parameters.

Diameter of hemispherical dome-shaped punch:	50mm
Blank material:	AA2014
Blank thickness:	1mm
Fixed and moved Plate Diameter:	150mm
Type of contact:	Forming one way surface to surface
Element type:	Rectangular and triangular
Blank element size:	3mm

The selection of measuring elements is as follows:

- The elements near the necking region are chosen randomly.
- Examining the true stress value, which corresponds to the Ultimate Tensile Stress value of the material, confirms the occurrence of a localized necking state.
- The simulation was continued until the equivalent stress value exceeded the true stress value corresponding to the ultimate tensile stress in cases where necking was not observed.

4 Results and discussions

4.1 Forming limit diagram (FLD)

The fracture histories of different specimen variants bulged at 0.1/s and at three temperatures (300°C, 150°C, and RT) were presented in Figure 5. During the Nakajima bulging process, the deformation of the specimens was measured using a stereo microscope. Post-processing analysis can reveal various stages of deformation, and the GOM-Correlate expert program can estimate the evolution of major and minor strains. It was discovered that the specimens with varying widths first underwent biaxial deformation before transitioning to a linear direction. The curvature of the hemispherical punch causes deviations from the ideal linear strain paths. Forming limit diagrams (FLD) are usually obtained along with linear strain paths. The Nakajima test involves the punch making initial contact with the center of the specimen. The contacting zone starts bulging with the biaxial tension strain path when the surrounding non-contacting area remains undeformed. As the punch moves, the contacting

region expands until it reaches full contact with the specimen, leading to a linear strain path that progressively develops, corresponding to the biaxial pre-strain route.

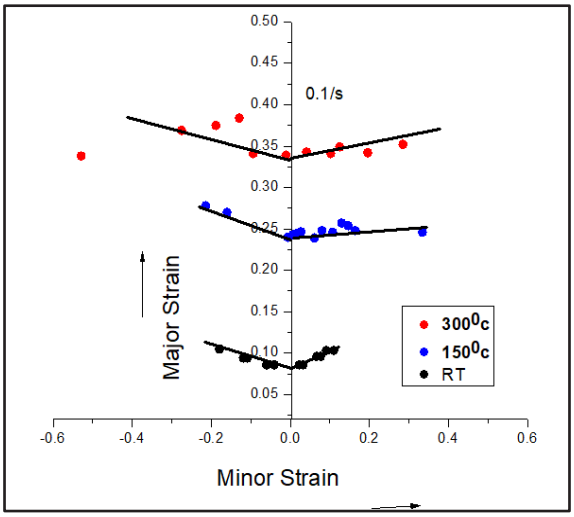

Fig.5. FLD for different temperatures 300,150 and RT

The measure of the major axis and minor axis length is taken at necking, failure, and safe region. Necking is a kind of defect that happens when a metal sheet is excessively stretched in a particular area, causing it to become thinner and decrease its overall area. It often occurs in sheet metal shaping procedures where the metal undergoes intense stresses and deformation rates. The repercussions of necking can be significant, impacting the malleability and strength of the metal sheet. Once a material necks, it undergoes a localized thinning, which can cause it to crack, tear, or even rupture. This defect can adversely affect the final product's quality, leading to an elevated risk of part malfunction or failure.

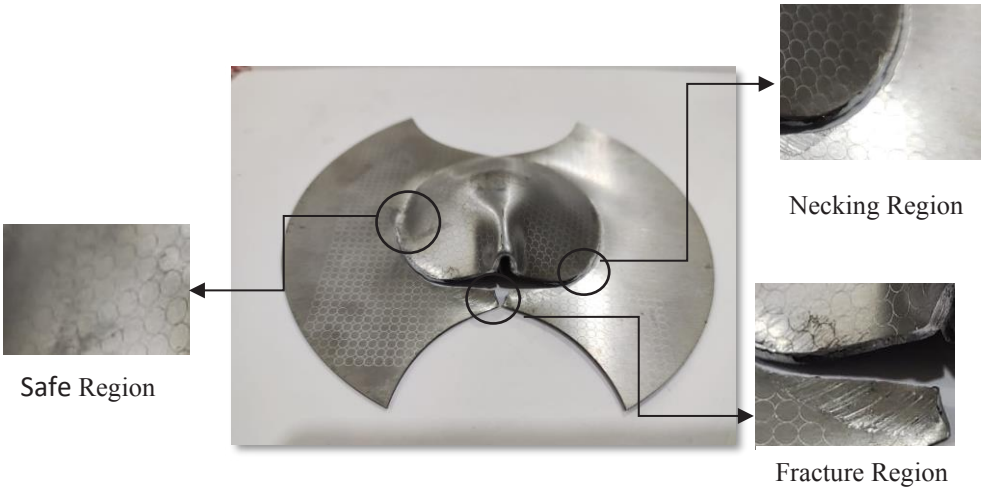

Fig.6. Necking, Failure, and Safe Regions of The Dome-Shaped Specimen

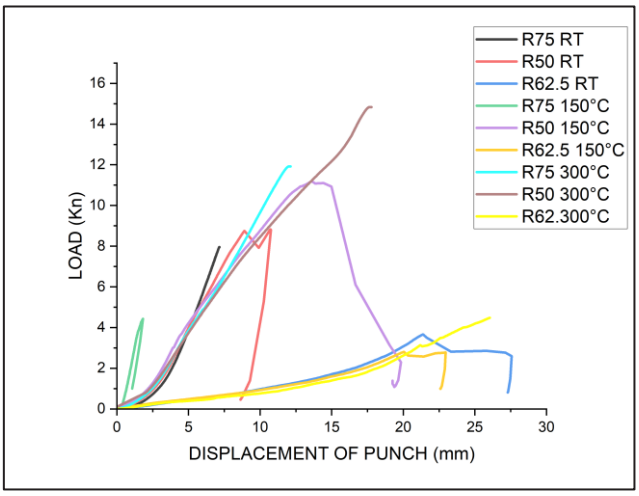

Fig.7. Load vs Displacement graph

4.2 Limiting dome height.

Limiting dome height (LDH) is a crucial metric for understanding how easily different specimens may be drawn at various temperatures. LDH is the height of the specimen at the moment of the impending fracture. The figure depicts how average LDH changes with temperature. Due to the material's thermal softening, LDH was observed to be rising as the test temperature increased. LDH is a critical factor in sheet metal forming and is influenced by factors such as the material's ductility, strain hardening, thickness, and grain structure. LDH plays a crucial role in designing sheet metal forming processes and selecting appropriate materials for specific applications.

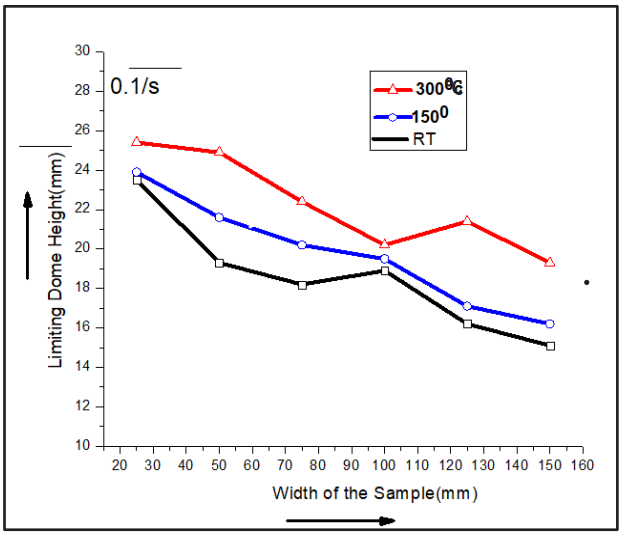

Fig.8. variation of LDH

4.3 Analysis of AA2014

The purpose of this research is to determine the correlation between predicted limit strains obtained through finite element simulations and those developed through experiments. The study involved simulating three different specimens subjected to various tension states at 150°C, which resulted in specific points on the forming limit diagram (FLD). Table 4 displays the major and minor strains obtained from simulations and experiments, while Figure 10 illustrates the deformed geometries of the three specimens at 150°C. The minor and major strains of each element were recorded according to the previously discussed selection criteria.

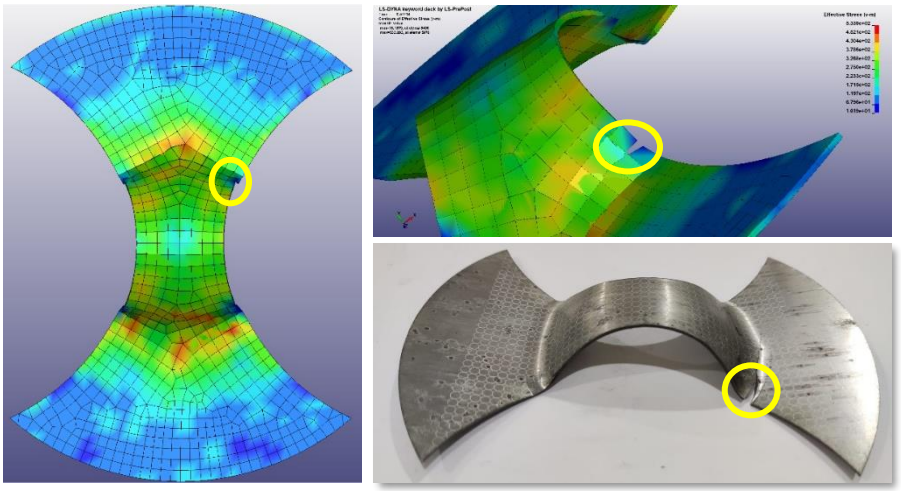

Fig.9. comparison between the experimental sample and simulation result.

The Nakazima test for AA 2014 specimens was simulated using LS Dyna finite element software, and the measuring elements were chosen as previously discussed. The resulting major and minor strain values of the elements were collected and plotted on a Forming Limit Curve (FLD) graph to determine the FLC of AA 2014.

Table 4. Experimental and FEM results

Specimen Dimensions (mm)	**Experimental results**		**Simulation Results**	
	Major Strain	**Minor Strain**	**Major strain**	**Minor Strain**
R75	0.24	0.31	0.28	0.33
R62.5	0.21	-0.18	0.23	-0.21
R50	0.16	-0.01	0.14	-0.03

The experimental and software-generated FLCs show a high degree of conformity with minimal discrepancies, indicating that the outcomes achieved through experiments are significant.

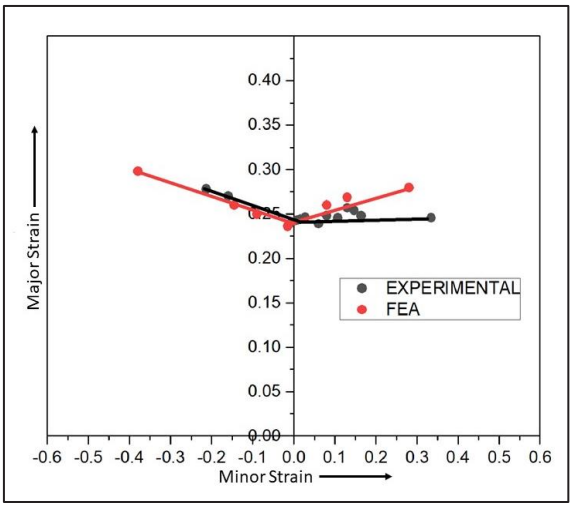

Fig.10. FLD generated by experiment and FEA.

The results of von mises stress effective plastic deformation and Resultant deformation are taken from the simulations. The von Mises stress, which is also referred to as equivalent or distortion energy stress, is a method of determining the maximum stress that a material can handle prior to experiencing plastic deformation. The von Mises stress considers both normal and shear stresses acting on a material, and its computation is based on the three-dimensional stress tensor. This stress measurement is an effective tool for predicting material failure and designing structures capable of withstanding anticipated loads.

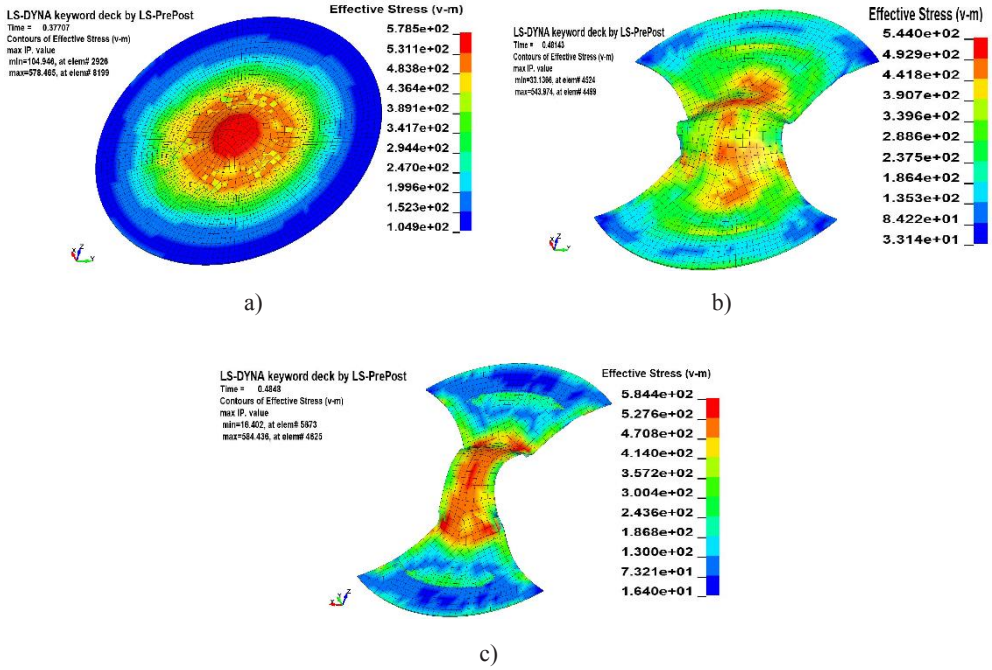

Fig.11. Simulations result of effective stress a) R75; b) R50; c) R62.5.

The analysis revealed that the 62.5 geometry had the highest effective stress as shown in figure 11. The area where the punch contacts the specimen experiences the maximum effective stress, while the non-forming region experiences the lowest. The effective stress increases with increasing deformation until the point of fracture.

Effective plastic strain is a metric that quantifies the plastic deformation that a material undergoes when subjected to mechanical loading. It differs from total plastic strain, which considers all plastic deformation that occurs throughout the material, as effective plastic strain only measures the plastic deformation in regions where the material has yielded beyond its elastic limit. This parameter is vital in determining the material's behaviour under load, as it can be utilized to forecast factors like material failure, fatigue, and overall durability. Engineers and scientists use various testing methods, such as tensile and compression tests, to gauge effective plastic strain, which helps them understand how materials behave under stress and design more resilient structures and products. The permanent deformation caused by the material being pushed beyond its elastic limit is considered an effective plastic strain.

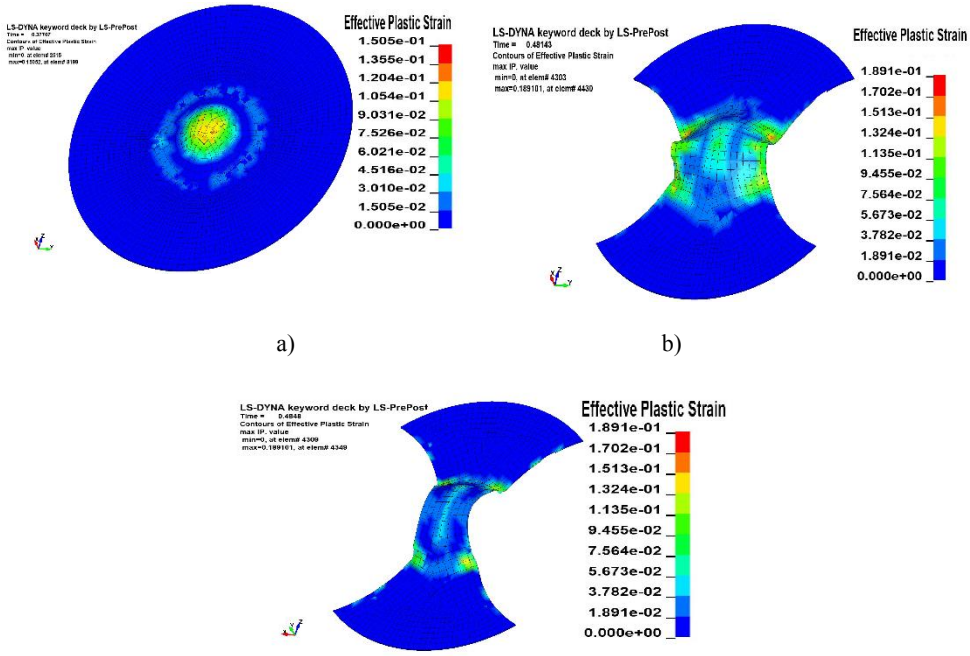

Fig.12. Simulations result of Effective plastic strain a) R75; b) R50; c) R62.5.

Based on the simulation results as shown in figure 12, it was observed that the R50 geometry resulted in the highest effective plastic strain (EPS), and the maximum EPS value for R62.5 and R75 was found at the centre of the geometry. For the R50 shape, the maximin EPS was found at the edges of the dome shape. Furthermore, it was noted that an increase in deformation led to an increase in EPS.

The resultant displacement in finite element analysis refers to the total displacement of a structure or element resulting from applied loads or given time. It is computed by solving a set of equations that depict the structure's behaviour under given loading circumstances. The magnitude and direction of the resultant displacement can be determined and used to evaluate the overall deformation and stability of the structure. Accurate computation of the resultant

displacement is crucial in engineering design to ensure that the structure can withstand intended loads and remain intact over time. Finite element analysis software is typically used to perform these computations and can provide detailed information on the behaviour of intricate structures under various loading scenarios.

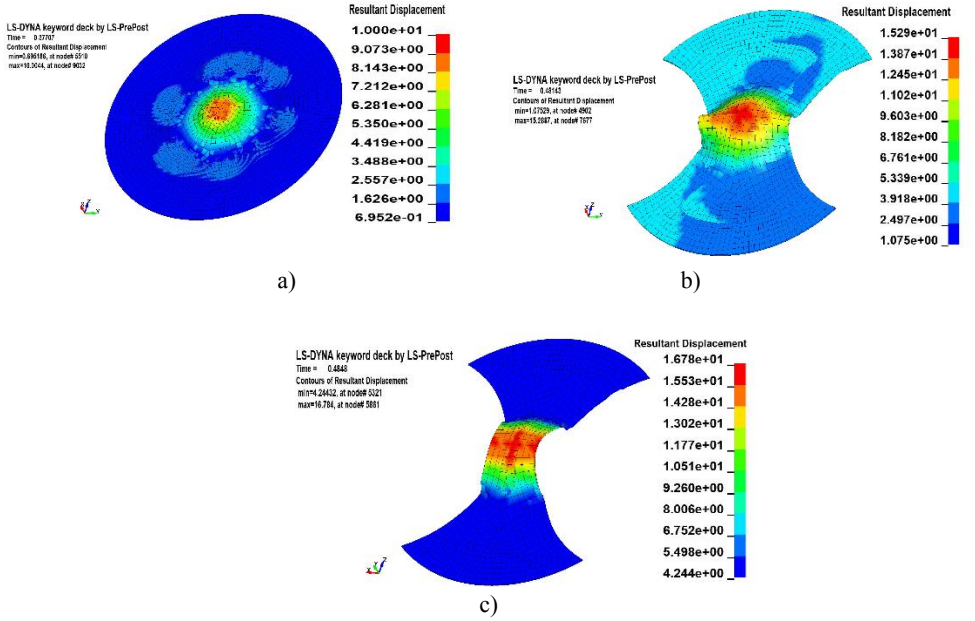

Fig.13. Simulations result of resultant displacement a) R75; b) R50; c) R62.5.

The punch displacement is greater for the R63.5 specimen as shown in figure 12, reaching 18.39mm. This is because of its particular shape, which causes an increase in stress as the punch displacement increases. Both simulation and experimental results show similar punch displacement values.

4.4 Microstructure Analysis

Scanning Electron Microscopy (SEM) is a powerful tool in fractography studies that enables detailed surface analysis of fractured materials. Fractography is the study of the fracture surfaces of materials to determine the underlying cause of failure. The material possesses a fine-grained and uniform structure with alloying elements distributed evenly throughout the material. However, at a microscopic level, the alloy exhibits a more intricate structure consisting of different phases. The primary phase is the α-Al matrix, responsible for the alloy's strength and ductility. From Figures (14,15,16) it can be clearly observed a ductile type of fracture in all cases of the study.

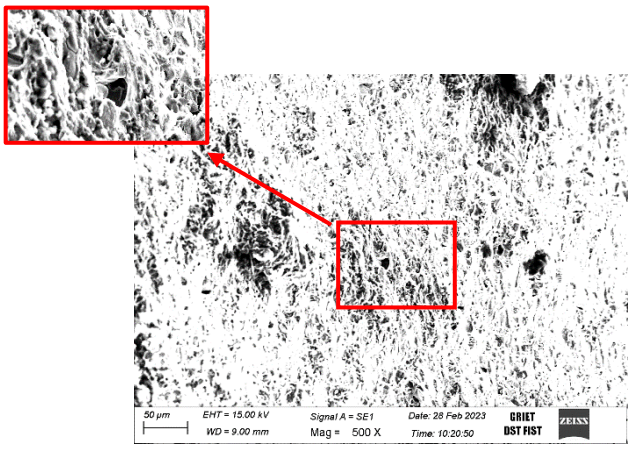

Fig.14. Fracture surface of R62.5 at room temperature

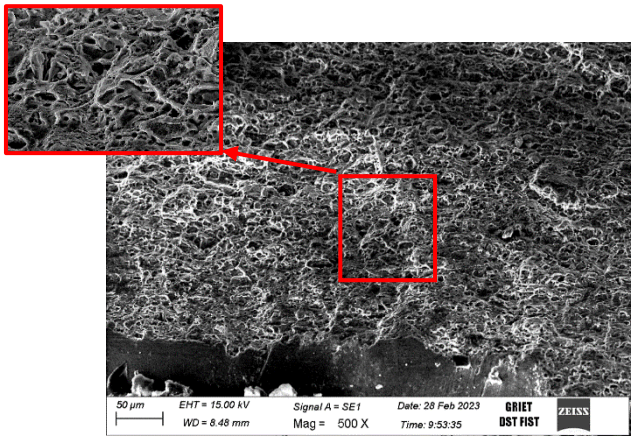

Fig.15. Fracture surface of R62.5 at 150°C

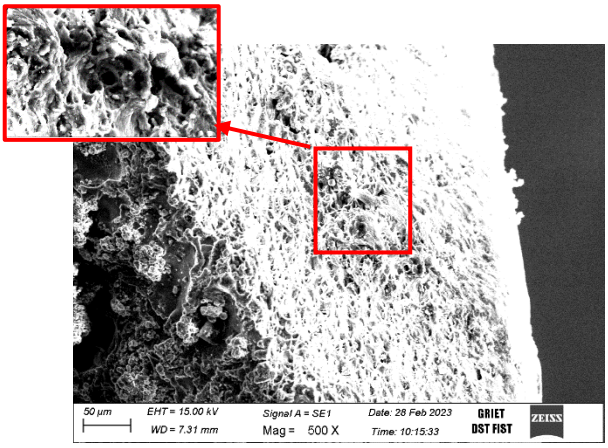

Fig .16. Fracture surface of R62.5 at 300°C

5 Conclusion

- The current study on AA 2014 aims to establish the forming limits at various temperatures using both experimental and FE Simulations. The study has produced several key findings, which are summarized below.
- Forming behaviour of AA2014 alloy has been investigated using the Nakajima test process from room temperature to 300℃ at an interval of 150℃.
- Forming Limit Diagram (FLD) has been determined experimentally for AA2014 at room temperature, 150℃, 300℃.
- FLD generated using the LS dyna simulation tool is compared with experimental FLD at 150℃ and it was observed the minimum error between them.
- It has been observed that AA2014 alloy is difficult to draw up to 150℃ and LDH was observed to be rising as the test temperature increased.
- Failure and necking were observed on the dome-shaped cups.
- From microstructure analysis clearly observed a ductile type of fracture in all cases of the study

References

1. Jürgen HIRSCH, Transactions of Nonferrous Metals Society of China, Volume 24, Issue 7, July 2014.
2. Tolga Dursun, Costas Soutis, Materials & Design (1980-2015) Volume 56, April 2014.
3. Rajiv S. Mishra, Harpreet Sidhar, Book-Physical Metallurgy of 2XXX Aluminium Alloys, Friction Stir Welding of 2XXX Aluminium Alloys Including Al-Li Alloys, 2017.
4. B. J. Varghese and P. B. Bobba, "Design and analysis of a robust system for wirelessly powering implantable devices," 2016 IEEE 1st International Conference on Power Electronics, Intelligent Control and Energy Systems (ICPEICES), Delhi, India, 2016, pp. 1-5,
5. S. P. Ringer, T. Sakurap And I. J. Polmear, Acta Materialia, Volume 45, Issue 9, September 1997.
6. M.A.M. Arif, M.Z. Omar Z. Sajuri, M.S. Salleh , Transactions of Nonferrous Metals Society of China, Volume 30, Issue 2, February 2020
7. Prasad, K.S., Gupta, A.K., Singh, Y., Singh, S.K., A Modified Mechanical Threshold Stress Constitutive Model for Austenitic Stainless Steels, Journal of Materials Engineering and Performance, 2016, 25(12), pp. 5411–5423
8. Gang CHEN, Tao ZHOU Bo WANG, HoHong-WeiIU, Fei HAN Transactions of Nonferrous Metals Society of China, Volume 26, Issue 1, January 2016.
9. Abass Ali Saleh , Contemporary Engineering Sciences, Vol. 11, 2018.
10. Naik, R.B., Ratna, D., Singh, S.K., Synthesis and characterization of novel hyperbranched alkyd and isocyanate trimer based high solid polyurethane coatings, Progress in Organic Coatings, 2014, 77(2), pp. 369–379
11. K. Ashok, K. Maruthupandian, K. Ganesh Kumar, C. Sundar Vishal, , Transactions of the Indian Institute of Metals volume 68, pages19–24 (2015).
12. Anoop Kumar Pandouria, Kuldeep Yadav, Vikrant Tiwari, Structures, Volume 49, March 2023.
13. Singh, S.K., Tambe, S.P., Raja, V.S., Kumar, D., Thermally sprayable polyethylene coatings for marine environment, Progress in Organic Coatings, 2007, 60(3), pp. 186–193.

14. Surajit Kumar Paul, The Journal Of Strain Analysis For Engineering Design, Volume 48 Issue 3, April 2013.
15. Baloji Dharavath, Ayush Morchhale, Nitin Kotkunde, Swadesh Singh, Journal of Materials Engineering and Performance, Volume 29, July 2020.
16. Sandeep Pandre, Ayush Morchhale, Nitin Kotkunde & Swadesh Kumar Singh (2020) Influence of processing temperature on formability of thin-rolled DP590 steel sheet, Materials and Manufacturing Processes, 35:8, 901-909
17. Syed Mujahed Hussaini, Geetha Krishna, Amit Kumar Gupta, Swadesh Kumar Singh, Journal of Manufacturing Processes, Volume 18, April 2015.
18. Xugang Wang , Xiaobo Fan , Xianshuo Chen , Shijian Yuan , Journal of Materials Processing Technology Volume 306, August 2022
19. Karthik Rao, R., Bobba, P.B., Suresh Kumar, T., Kosaraju, S., Feasibility analysis of different conducting and insulation materials used in laminated busbars, Materials Today: Proceedings, 2019, 26, pp. 3085–3089
20. Lade Jayahari, P.V. Sasidhar, P. Prudvi Reddy, B. BaluNaik, A.K. Gupta, Swadesh Kumar Singh, Formability studies of ASS 304 and evaluation of friction for Al in deep drawing setup at elevated temperatures using LS-DYNA, Journal of King Saud University - Engineering Sciences, Volume 26, Issue 1, 2014, Pages 21-31.
21. J Pavan Kumar, R Uday Kumar, B Ramakrishna, B Ramu and K Baba Saheb 2nd International Conference on Advancements in Aeromechanical Materials for Manufacturing, volume 455,july 2018.
22. Nejia Ayachi , Noamen Guermazi , Cong Hanh Pham . Metals 2020, 10(9), 116, august 2020.
23. Tummala, S.K., Indira Priyadarshini, T., Morphological Operations and Histogram Analysis of SEM Images using Python, Indian Journal of Engineering and Materials Sciences, 2022, 29(6), pp. 794–798.
24. L. Venugopal, M. J. Davidson & N. SelvarajMaterial and manufacturing process, volume 28, issue 3,2013.
25. Suresh Kumar Tummala, Phaneendra Babu Bobba & Kosaraju Satyanarayana (2022) SEM & EDAX analysis of super capacitor, Advances in Materials and Processing Technologies, 8:sup4, 2398-2409
26. Nitin Kotkunde , Amit Kumar Gupta a, Prudvi Reddy Paresi , Swadesh Kumar Singh, Materials Today: Proceedings Volume 4, Issue 4, 2017.
27. Lumelskyj a, J. Rojek a, L. Lazarescu b, D. Banabic , Procedia Manufacturing, Volume 27, 2019,
28. B. J. Varghese, P. B. Bobba and M. Kavitha, "Effects of coil misalignment in a four coil implantable wireless power transfer system," 2016 IEEE 7th Power India International Conference (PIICON), Bikaner, India, 2016, pp. 1-6
29. Sreenath D Kumar, Amjith T.R, C. Anjaneyulu, Procedia Technology, Volume 24, 2016.
30. J.J.S. Dilip, G.D. Janaki Ram, Materials Characterization, volume 86, December 2013